A 180 GHz to 220 GHz Wideband Transmitarray with Wide-Angle Beam Steering for Intersatellite Communications

Li-Zhao Song, Ting Zhang, Jie-Xin Lai, Yang Yang, and Jia Du

***Abstract*— This article presents a terahertz (THz) wideband transmitarray antenna with wide-angle beam steering for intersatellite communications. A new design method is developed for beam steering/multibeam transmitarrays based on feed displacement. The phase compensations on the transmitarray aperture are theoretically analysed for two steered symmetrical beams from two conjugate foci in an arbitrary azimuthal plane. Then, the focus for a boresight beam is investigated to minimise the corresponding phase errors. A circular feed track is produced with the three foci, enabling wide-angle and low-scanning-loss beam steering by changing the focal point. A unit cell model based on the Huygens metasurface is designed with only one substrate layer, capable of continuously tuning the phase in a 360° range with low transmission losses. The THz transmitarray prototype is engineered with the developed beam-steering method and unit cells. The prototype is experimentally verified with a wideband stable beam-steering performance from 180 GHz to 220 GHz in a wide angular range of ±48°. The measured minimal scanning loss is only 1.4 dB. The measured 3-dB gain bandwidth of the boresight beam is 19.1%.**

***Index Terms*— Beam steering, intersatellite communications, THz, transmitarray.**

I. Introduction

Low Earth Orbit (LEO) satellites have been playing an essential role in our society for global communications, Earth observations, navigations and Global Positioning System (GPS), as well as Internet of Things (IoT) [1]. The growing demands of services are posing great challenges to the satellite to exchange a mass of data with its linked ground station in real-time, since a satellite-ground connection is not continuous as it rotates around the Earth. To tackle this issue, intersatellite communications have been widely hailed for its capability of relaying data through adjacent satellites [2], as illustrated in Fig. 1. By establishing intersatellite links, efficient and timely data exchange can be promised when the satellite cannot directly contact a given ground station.

Meanwhile, THz antennas, operating in 0.1-10 THz, are particularly attractive for satellite communications thanks to their high data rates, high security and low interference [3]. However, THz antennas usually feature high gains to compensate for their high propagation losses, causing small beam coverages. Therefore, beam-steering capability is highly desired for THz antennas to support stable communication links between constantly moving satellites. Two typical methods have been widely investigated for THz beam steering, namely, phased-array-based electrical steering [4]-[5] and mechanical steering with spatial-shifting mechanisms [6]-[8]. When the steering speed is not a major factor, mechanical steering has its unique merits of low loss, low complexity and high gain with flexibility on large-aperture implementations. To this end, transmitarray/reflectarray antennas are competitive candidates for THz beam steering due to their simple configurations and flexible wave manipulations using various mechanical steering methods [9]-[11].

To date, most advances for beam-steering transmitarray/reflectarray antennas were reported at microwave bands [12]-[26]. Among different mechanisms, the method of displacing feed sources relatively to the array aperture is particularly attractive due to its potential for multibeam radiations when multiple feeds are applied simultaneously [12]-[24]. This will also enable its applicability for satellite-to-multi-satellite communications. Within this scope, different techniques have been developed to enlarge the beam coverage and reduce the scanning loss. In [12], a multibeam phase

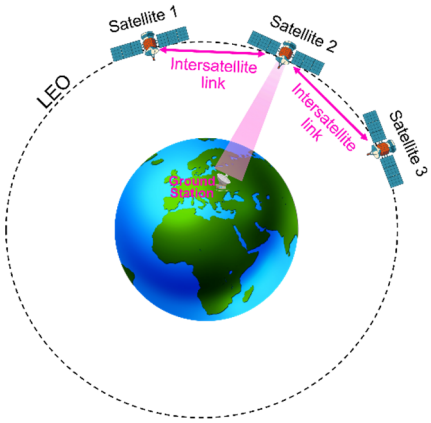

Fig. 1. Diagram of intersatellite communications.

matching method for reflectarrays was developed to synthesise aperture phase distributions for multiple beams based on algorithm optimisations of feed offset angles and reference phases. A wide beam-steering range of ±45° was obtained with a low scanning loss of 1.7 dB at 12 GHz. In [20], a dual-band transmitarray was designed for beam steering at 19.5 GHz and 29 GHz based on a bifocal phase compensation method. Beam coverages of ±40° and ±30° have been obtained with the same scanning loss of 2 dB at the two centre frequencies, respectively. In [23], offset unifocal phase symmetry was proposed to improve the beam-steering performance of transmitarrays from the bifocal method. A beam coverage of ±30° was realised with a low scanning loss of 1.6 dB at 25 GHz. Based on the reported beam-steering methods with the feed displacement mechanism in literature, it is found that the transmitarrays still face challenges of achieving larger than ±45° coverages and less than 3-dB scanning losses. Many reported transmitarrays/reflectarrays with advanced beam-steering performances would rely on optimisation algorithms with iterative retrieval processes. A comprehensive and highly reliable analytical method with straightforward design formulas for wide-angle, low-scanning-loss beam steering/multibeam radiations is still in demand, especially for transmitarrays. In [24], an elliptically shaped multibeam transmitarray was analytically elaborated for a wide beam coverage of ±43° with a scanning loss of 2.7 dB at 70.5 GHz. However, this shaped structure will affect the practical implementations on planar platforms and limit its applications.

This work presents a new design methodology for planar wide-angle mechanical beam-steering/multibeam transmitarrays based on the feed displacement mechanism. Distinct from the bifocal method using averaged aperture phase distributions of two independent beams [21], this work finds a new solution for the aperture phase modulation that can directly enable two symmetrical beam radiations. Besides, phase errors for the boresight beam are analysed and can be minimised. Explicit design formulas for both aperture and feed configurations are derived to support wide-angle beam steering. A Huygens unit cell on a single substrate layer facilitates phase manipulations on the aperture. Finally, a THz wideband transmitarray with wide-angle beam steering and low scanning loss has been demonstrated for the first time. It shows superior performance compared to other THz mechanical beam-steering designs.

Furthermore, in contrast to the reported transmitarrays at microwave band, this work can enable a wider beam coverage and a lower scanning loss without resorting to optimisation algorithms.

II. Methodology for Wide-Angle Beam-Steering Transmitarrays

We aim to design a beam-steerable transmitarray without changing its aperture configuration. The beam can be steered from different feed locations. As illustrated in Fig. 2, the transmitarray (in the *xoy* plane) with an offset focal point (Feed A) is initially investigated for an oblique radiation beam. We consider the feed position and radiation beam to be in the same azimuthal plane, e.g., φ=φ_0 plane in Fig. 2. Feed A has a focal length of d_0 and an elevation angle of θ_0, with a polar coordinate of (d_0, θ_0, φ_0). The radiation beam has an elevation angle of θ_r.

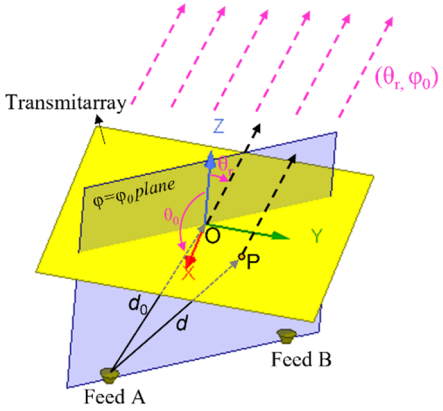

Fig. 2. Beam-steerable transmitarray with offset illuminations.

Therefore, the phase compensation of a random point P at the position of (x, y) on the transmitarray aperture can be calculated from

$$k_0 d_0 + \Delta\varphi + k_0 \sin\theta_r (x\cos\varphi_0 + y\sin\varphi_0) = k_0 \sqrt{(x - d_0 \sin\theta_0 \cos\varphi_0)^2 + (y - d_0 \sin\theta_0 \sin\varphi_0)^2 + (d_0 \cos\theta_0)^2}, \quad (1)$$

where k_0 is the free-space propagation constant, $\Delta\varphi$ represents the relative phase compensation at the point P with respect to the origin.

In order to enable wide-angle beam steering, another conjugate feeding scenario is investigated, wherein the transmitarray is illuminated by Feed B in Fig. 2. The location of Feed B is symmetrical to the one of Feed A in φ=φ_0 plane, with a polar coordinate of (d_0, -θ_0, φ_0). Correspondingly, the radiation beam is desired as symmetrical to the previous one, with a direction of (-θ_r, φ_0). Another phase compensation formula from the new focal point (Feed B) can be obtained as

$$k_0 d_0 + \Delta\varphi - k_0 \sin\theta_r (x\cos\varphi_0 + y\sin\varphi_0) = k_0 \sqrt{(x + d_0 \sin\theta_0 \cos\varphi_0)^2 + (y + d_0 \sin\theta_0 \sin\varphi_0)^2 + (d_0 \cos\theta_0)^2}. \quad (2)$$

If considering given desired beam directions (±θ_r, φ_0) and focal length d_0, there are only two unknowns from (1)-(2), i.e., the relative phase compensation $\Delta\varphi$ and the feed elevation angle θ_0. Consequently, through mathematical derivations, they can be solved as

$$\Delta\varphi = -k_0 d_0 + k_0 \sqrt{d_0^2 - [\sin^2\theta_r (x\cos\varphi_0 + y\sin\varphi_0)^2 - x^2 - y^2]}, \quad (3)$$

$$\theta_0 = \arcsin(-\sin\theta_r (1 + \frac{\Delta\varphi}{k_0 d_0})) = \arcsin(-\sin\theta_r \sqrt{1 - \frac{[\sin^2\theta_r (x\cos\varphi_0 + y\sin\varphi_0)^2 - x^2 - y^2]}{d_0^2}}). \quad (4)$$

It is noticed from (4) that the calculated elevation angle of feed positions is not a fixed value. Instead, it is a variable related to different points on the transmitarray aperture. As an example, considering the desired radiation beams at (±θ_r=±48°, φ_0=0°), the solutions of (4) with respect to different points on the aperture can be plotted, as in Fig. 3. It ranges from -132° to -127.5° with a less than 5° variation. Besides, the large variations appear only at the edges of the aperture. Therefore, one can adopt an average value to fix the feed position as

$$\theta_0 = \text{mean}(\arcsin(-\sin\theta_r (1 + \frac{\Delta\varphi}{k_0 d_0}))). \quad (5)$$

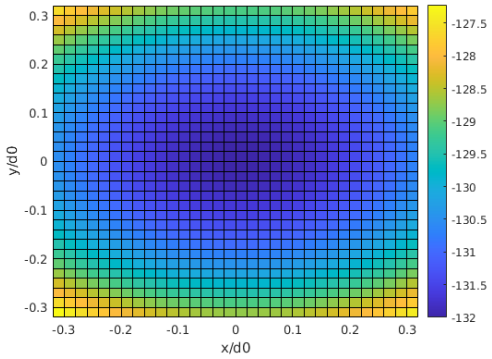

Fig. 3. Theoretical feed elevation angles versus positions on the transmitarray.

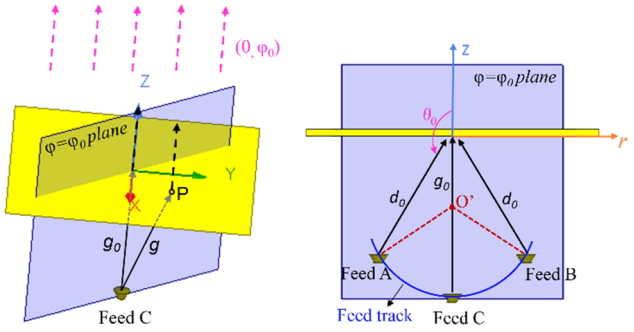

Fig. 4. (a) Beam-steerable transmitarray with illuminations from Feed C for a boresight beam. (b) Feed arrangement in the azimuthal plane of beam steering.

Based on the above derivations, the transmitarray can enable two symmetrical oblique beam radiations from the two calculated offset feed positions. However, the feed for a boresight beam is also crucial to enable steerable beams. As shown in Fig. 4 (a), the transmitarray is illuminated by Feed C, located on the negative z-axis with a focal length of g_0. To achieve the boresight beam, the required relative phase compensation at point P should be

$$\Delta\varphi_1 = -k_0 g_0 + k_0 \sqrt{g_0^2 + x^2 + y^2}. \quad (6)$$

Since the phase compensations on the aperture have already been determined from (3) for the two oblique beams, the phase errors for the boresight beam will be

$$\delta = |\Delta\varphi - \Delta\varphi_1| = |k_0(g_0 - d_0) + k_0(\sqrt{d_0^2 - [sin^2\theta_r(x\cos\varphi_0 + y\sin\varphi_0)^2 - x^2 - y^2]} - \sqrt{g_0^2 + x^2 + y^2})|. \quad (7)$$

For different values of g_0, the phase errors on the transmitarray will be different. Therefore, g_0 should be chosen for a good boresight radiation when the phase errors are minimal. For further analysis, (7) can be approximated by Taylor series expansions for two variables of x and y around the aperture centre (0, 0), leading to

$$\delta \approx x^2 k_0\left(\frac{1}{2g_0} - \frac{1-\cos^2\varphi_0\sin^2\theta_r}{2d_0}\right) + y^2 k_0\left(\frac{1}{2g_0} - \frac{1-\sin^2\varphi_0\sin^2\theta_r}{2d_0}\right) + \frac{k_0 xy\cos\varphi_0\sin\varphi_0\sin^2\theta_r}{d_0}. \quad (8)$$

For a simpler analysis, here we consider the beam steering plane as the *xoz* plane, i.e., φ_0=0°. In this case, (8) can be simplified as

$$\delta \approx x^2 k_0\left(\frac{1}{2g_0} - \frac{\cos^2\theta_r}{2d_0}\right) + y^2 k_0\left(\frac{1}{2g_0} - \frac{1}{2d_0}\right). \quad (9)$$

From (9), it is noticed that there is no single solution of g_0 that can satisfy δ=0 for all points on the aperture, i.e., arbitrary values of x and y. However, we can minimise the phase errors along the beam-steering plane and its orthogonal plane, respectively, i.e., the *xoz* plane (y=0) and the *yoz* plane (x=0). Specifically, the phase errors along the beam-steering plane will be 0 only if $g_0=d_0/\cos^2\theta_r$. On the other hand, the phase errors along its orthogonal plane will be 0 only if $g_0=d_0$. Therefore, the value of g_0 should be chosen within the range of [d_0, $d_0/\cos^2\theta_r$] to compromise phase errors along the two planes. It should be noted that the above analysis and the calculated range of g_0 also applies in the cases when the beam steering plane is not *xoz* plane ($\varphi_0\neq$0°) based on (8). It is not elaborated here due to limited space. The determination of g_0 for a fixed value will be shown in a specific transmitarray design in Section IV.

With the calculated offset feed positions (Feeds A and B) and a determined Feed C position, a feed track can be subsequently produced in the beam-steering azimuthal plane ($\varphi=\varphi_0$) with an arc shape, as in Fig. 4 (b). Its pivot is at O'. By sliding the feed source along the feed track, continuous beam steering can be achieved between $\pm\theta_r$.

III. Unit Cell

A Huygens unit cell is developed to implement phase compensations on the transmitarray aperture, as shown in Fig. 5 (a). Compared to other unit cell types, e.g., frequency selective surfaces (FSS) and receiver-transmitter models, the Huygens unit model can be realised with only two metallic layers on a single substrate without any metallic vias. This will simplify the fabrication process and mitigate performance deviations at THz frequencies. Two metallic layers are printed on Rogers RT/Duroid 5880 with a thickness of h=0.254 mm. It has an effective permittivity of ε_r=2.3 and a high loss tangent of 0.02 at 200 GHz [27]. The top and bottom layers have the same metallic pattern yet are mirrored along the x-axis. Each layer includes two split square rings. There is an overlapped part from the top and bottom layers, as illustrated in Fig. 5 (d). This unit cell is based on the Huygens metasurface concept [28]-[29]. Considering y-polarisation waves, the whole metal strips along the y-axis will contribute to electric responses, while the overlapped parts will produce magnetic responses. The periodicity of the unit cell is S=0.75 mm. The two split rings have the same width of w=0.05 mm. The lengths along the x-axis of the two rings are denoted as L_1 and L_2, respectively. The lengths along the y-axis are denoted as d_1 and d_2, respectively. Considering the fabrication tolerance for the gap between two rings, we define L_2=L_1-0.2 mm.

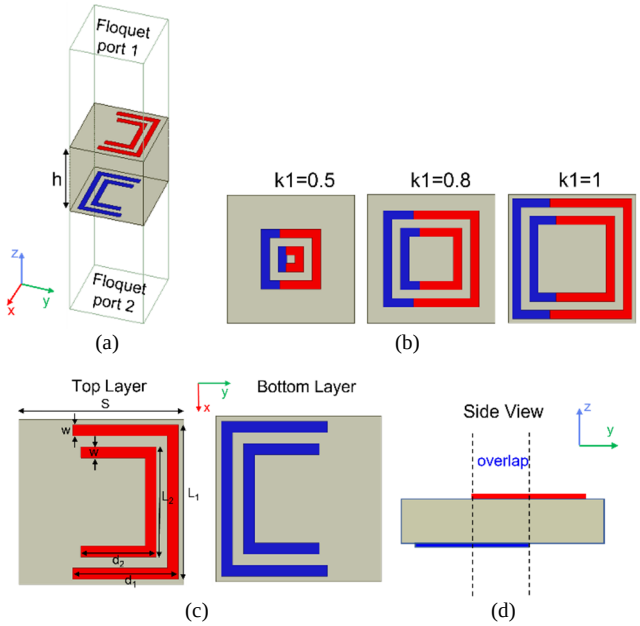

Fig. 5. Sketch of the unit cell (Bule and red colours represent bottom and top metals, respectively). (a) 3D model. (b) Top view of unit cells with different dimensions. (c) Top and bottom layers. (d) Side view.

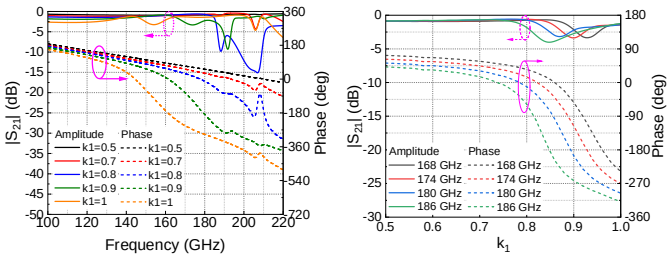

Fig. 6. (a) Transmission coefficients versus frequency. (b) Transmission coefficients versus the factor k_1 at different frequency points.

For S-parameter characterisations, periodic boundaries in ANSYS HFSS are assigned along both x- and y-axes, and two Floquet ports are added along z-axis. After parametric studies, the final dimensions of the metallic layer are: L_1 = 0.7k_1 mm, d_1=0.48 k_1 mm and d_2=0.686L_2=0.686(L_1-0.2) mm. A factor k_1 is involved and varied consecutively from 0.5 to 1 to enable transmission phase tuning. To visualise different shapes of unit cells, three of them with different dimensions are shown in Fig. 5 (b). The simulated transmission amplitudes and phases for different unit cells under y-polarisation incidence are plotted in Fig. 6 (a). It is observed that a transmission band up to 186 GHz has been realised with a maximal transmission loss of 3.3 dB. The surface current distributions of the unit cell with k_1=1 at 180 GHz are shown in Fig. 7 for different times in one period of T. The surface currents on each pair of y-axis strips of the top and bottom layers show opposite directions at t=0 and t=T/2. As explained in [28]-[29], the overlapped strips from Fig. 5 (d) with opposite current directions can be regarded as a current loop, thereby mimicking magnetic responses. However, at t=T/4 and t=3T/4, the currents on each pair of strips have the same directions, contributing to electric responses. The alternating electric and magnetic responses support the function of Huygens metasurfaces. Fig. 6 (b) displays the transmission amplitudes and phases versus the factor k_1 at different frequency points. A full phase range of 360° has been achieved at 186

GHz by varying k_1 from 0.5 to 1. Since the applied substrate material exhibits a higher loss tangent at the THz band, the unit cell shows a higher transmission loss in contrast to the Huygens unit cell in the microwave band.

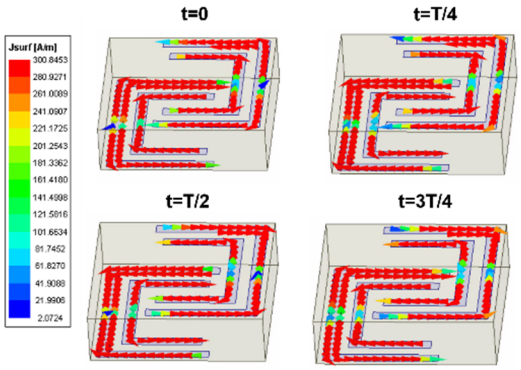

Fig. 7. Current distribution at 180 GHz within one time period.

IV. Beam-steering Transmitarray Design

A. Modelling and Simulation

To validate the developed beam-steering methodology in Section II, a transmitarray consisting of 30×30=900 unit cells is designed for wide-angle beam steering along *xoz* plane (φ_0=0). Referring to Fig. 2, a focal length of d_0=40 mm is chosen for the two symmetrical offset feeds to enable the maximal oblique beam angles at $\pm\theta_t$=±48°. The phase distributions on the transmitarray aperture are calculated from (3), as mapped in Fig. 8 (a). The aperture can be implemented by arranging phase-variable unit cells from Section III. The two offset feed positions are determined with their elevation angles calculated from (5), resulting in θ_0=-131°. As discussed in Section II, there are phase errors on the transmitarray if the boresight radiation is desired from a feed on the negative *z*-axis. Its focal length g_0 should be chosen within the range of $[d_0,\ d_0/\cos^2\theta_t]$ to balance phase errors along the beam-steering and orthogonal planes.

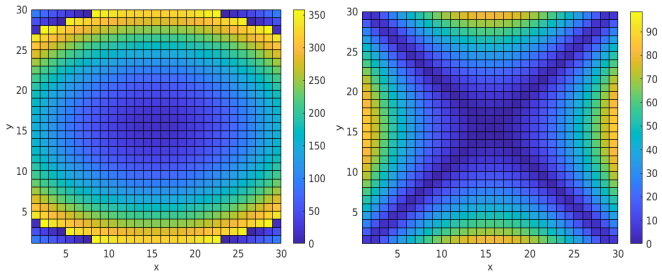

(a) (b)

Fig. 8. (a) Phase distributions on the transmitarray aperture. (b) Phase error distribution for g_0=55.6 mm.

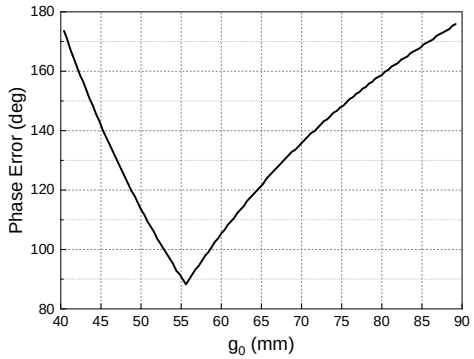

Fig. 9. Maximal phase errors on the transmitarray versus focal length g_0.

Here, we choose the optimal focal length considering the maximal phase error on the transmitarray aperture is the smallest. To this end, the maximal values of δ from (7) are analysed at 185 GHz under different g_0 within $[d_0,\ d_0/\cos^2\theta_t]$, i.e., [40, 89] mm. As given in Fig. 9, the minimal phase error occurs at g_0=55.6 mm. In this case, the corresponding phase error distribution is shown in Fig. 8 (b), where the maximal errors appear at the edges of the surface with values of around 88°. Besides, it is noticed that phase errors along *x*- and *y*-axes have been well balanced. It should be noted that the optimisation of g_0 is independent of frequency following (7)-(9). Only the absolute values of the phase error will be changed at different frequencies.

After the determinations of three focal points, i.e., Feeds A, B and C, the feed track with an arc shape can be obtained as in Fig. 4 (b). A conical horn antenna modelled based on a VDI prototype is applied here as the feed source. It has a waveguide size of WR-5.1 and operates from 140 GHz to 220 GHz. The realised gain is around 22 dBi at the centre frequency. By moving this conical horn along the feed track from Feed A to Feed B, wide-angle beam steering has been achieved. In Fig. 10 (a), the normalised radiation patterns from simulations at 185 GHz are provided, showing a wide beam-steering range of ±48°. Sidelobe levels are lower than -10 dB for all beams. Fig. 10 (b) shows the realised gains versus frequency regarding different beam directions. It is noticed that the simulated peak realised gain at 185 GHz is 29.2 dBi with a scanning loss of 1.8 dB. The scanning performance deteriorates with increasing scanning losses at above 185 GHz. This is owing to the limited bandwidth of the employed unit cell, as shown in Fig. 6 (a). To achieve consistent scanning performances at higher frequencies, a new unit cell covering a broader THz bandwidth should be deployed. This will be investigated in our future work.

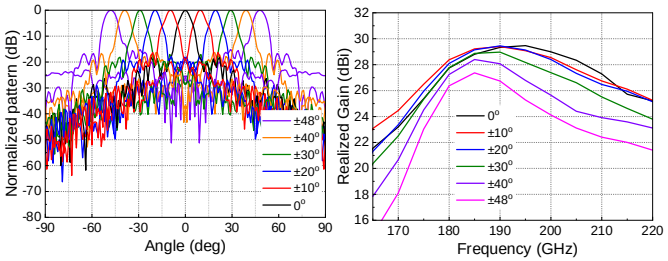

(a) (b)

Fig. 10. Simulation results. (a) Normalised radiation patterns at 185 GHz. (b) Realised gains of different beams versus frequency.

B. Fabrication and Measurement

As a proof of concept, the above-designed transmitarray prototype is fabricated based on printed circuit board (PCB) manufacturing using laser etching technology on the Rogers RT/Duroid 5880 substrate with a 0.254-mm thickness. Then, it is plated with gold to promise good conductivity at THz frequencies. The minimal realisable dimension of this fabrication process is 0.05 mm with a tolerance of ±0.005 mm. The fabricated prototype is shown in the inset of Fig. 11 (a). It is positioned on a rotatable base and fed by the conical horn on an adjustable platform for alignment. The feed horn is connected to a transmitter that can upconvert the frequency band to 170-260 GHz. A picture of the measurement setup is given in Fig. 11 (b). The transmitarray prototype with the transmitter is placed on a 3D-printed board that can be rotated along a circular track with the prototype as the pivot. Meanwhile, a horn antenna connected to a down-converting receiver is fixed on the optical table at the far field. The radiation patterns can be measured when rotating the board to different angles along the track.

The feed horn should be placed at different positions to demonstrate the beam-steering property, as illustrated in Fig. 4 (b). However, due

to the limited facility in our lab for a large movement of the horn together with the transmitter, we vary the relative position of the transmitarray instead. As shown in Fig. 11 (c), the transmitarray can be rotated around its centre with the rotatable base underneath. Besides, the focal length can be changed by linearly sliding the horn and transmitter on the adjustable platform. This way, each radiation beam from a specific feed position can be achieved by tuning the focal length l and the relative angle α of the transmitarray to the feed horn accordingly.

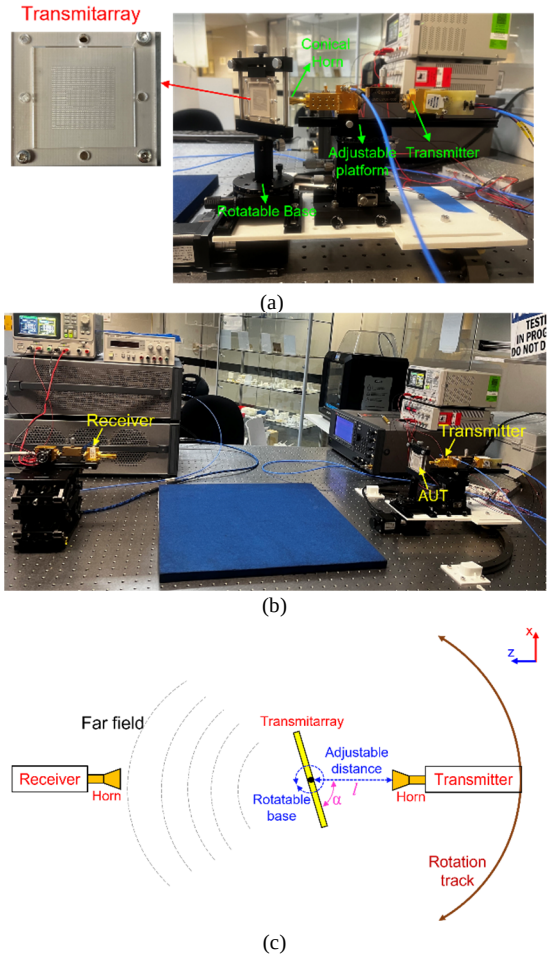

Fig. 11. (a) Transmitarray prototype. (b) Measurement setup. (c) Simplified diagram of the measurement setup.

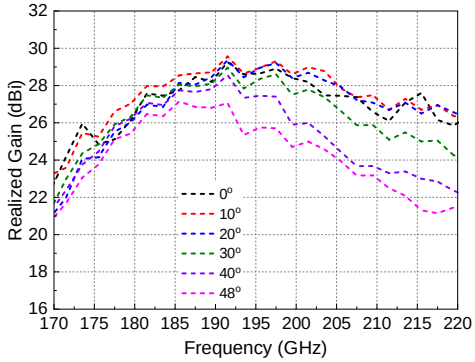

Fig. 12. Realised gain versus frequency of different beams from measurement.

The realised gains versus frequency from measurement for different beams are plotted in Fig. 12, showing a peak value of 29.6 dBi at 191.5 GHz for the beam of 10°. Due to the structural symmetry, only positive angles are provided. The measured 3-dB gain bandwidths for beams of 0°, 10°, 20°, 30°, 40° and 48° are 19.1% (179.5-217.5 GHz), 21.4% (177.5-220 GHz), 20% (180-220 GHz), 16.5% (177.5-209.5 GHz), 12.9% (177.5-202 GHz), and 14.7% (176-204 GHz), respectively. The beam scanning losses are between 1.4-4.3 dB from 177.5 GHz to 210 GHz. The radiation patterns at 200 GHz from both simulation and measurement are normalised in Fig. 13 (a). They agree with each other reasonably well with beam steering between ±48°. The relative cross-polarisation levels with respect to the corresponding co-polarisation levels are given in Fig. 13 (b), less than -30 dB for all different beams. The measured radiation patterns at 180 GHz, 190 GHz, 210 GHz and 220 GHz are normalised in Fig. 14 (a)-(d), respectively. It is noticed that consistent wide-angle beam steering has been realised in the operating frequency band.

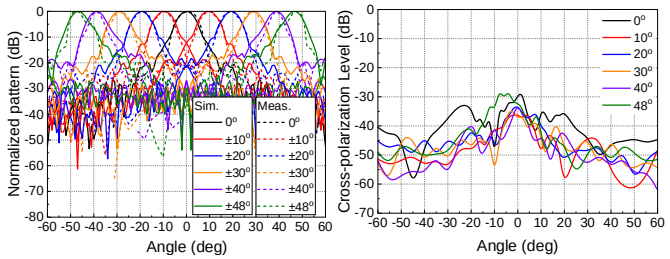

Fig. 13. Normalised patterns from simulation and measurement at 200 GHz. (b) Measured cross-polarisation levels of different beams at 200 GHz.

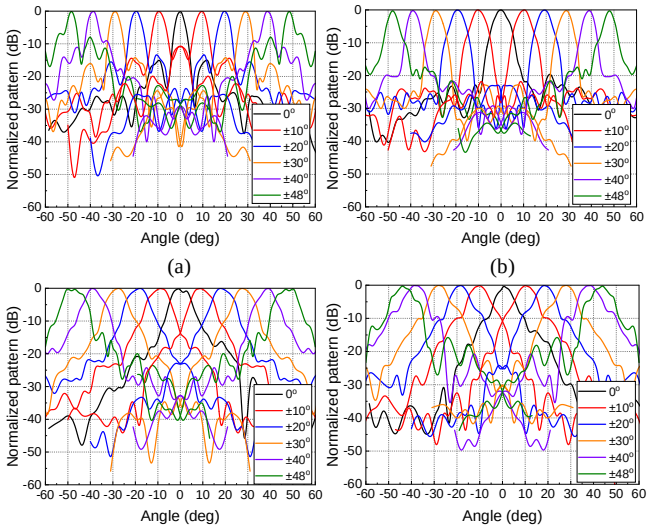

Fig. 14. Measured normalised radiation patterns. (a) 180 GHz. (b) 190 GHz. (c) 210 GHz. (d) 220 GHz.

To visualise the performance advances of the developed THz beam-steering transmitarray, a comparison table is produced as TABLE I including other reported mechanical beam-steering antennas at both microwave and THz bands. Please note that the beam range listed in TABLE I represents the angular coverage considering both beam steering and multibeam capabilities. Compared to the reported beam-steering/multibeam transmitarrays based on the feed displacement at microwave band, this work has realised a wider beam coverage and a low scanning loss without resorting to iterative optimisation algorithms. The beam-steering performance has been enhanced compared to other analytical methods. Moreover, this work represents the first implemented wide-angle beam-steering transmitarray antenna at THz band. In contrast to other THz mechanical beam-steering techniques, superior scanning performances have been obtained with a wider scanning range and a lower scanning loss.

TABLE I
COMPARISONS WITH OTHER REPORTED MECHANICAL STEERING DESIGNS

Ref.	Centre Freq. (GHz)	Design Method	Beam Range	Min. S.L. (dB)	3-dB G.B.	Peak A.E.
[6]	300	Luneburg Lens	50°	3	6.7%	/
[8]	180	Elliptical Lens	25°	3.6	44%	89%
[12]	12	Reflectarray (Algorithm)	90°	1.7	10% (1-dB)	43.1%
[19]	10	Transmitarray (Analytical Method)	60°	1.6	11%	37.4%
[20]	19.5/29	Transmitarray (Analytical Method)	80°/ 60°	2/2	11.8%/ 11.7%	11%/ 8%
[22]	30	Transmitarray (Algorithm)	50°	1.1	6.7% (1-dB)	20%
[23]	25	Transmitarray (Analytical Method)	60°	1.6	15.4%	28.5%
This work	**200**	**Transmitarray (Analytical Method)**	**96°**	**1.4**	**19.1%**	**35%**

***** Min. S.L. = Minimal Scanning Loss, G.B. = Gain Bandwidth, A.E. = Aperture Efficiency.

V. CONCLUSION

This work presents a THz beam-steering transmitarray antenna operating from 180 GHz to 220 GHz for intersatellite communications. A new beam-steering methodology, including newly derived phase compensation equations accompanied by a circular feed track, is developed to enable wide beam coverages and low scanning losses. A transmitarray prototype based on single-substrate-layer Huygens unit cells is designed and analysed, showing good simulation and measurement results. A wide beam-steering range of ±48° has been achieved with a minimal scanning loss of 1.4 dB. The measured peak realised gain can reach 29.6 dBi at 191.5 GHz. The 3-dB gain bandwidth is 19.1% for the boresight radiation. Consistent wide-angle beam steering has been observed in the whole operating band. It should be noted that this work can only support 1-D beam steering. Further analyses should be conducted for 2-D beam steering by involving more research knowledge, such as optimisation algorithms.

REFERENCES

[1] R. Cochetti, "Mobile satellite communications handbook," *John Wiley & Sons*, Sep. 2014.

[2] P. Wang, H. Li, B. Chen and S. Zhang, "Enhancing earth observation throughput using inter-satellite communication," *IEEE Trans. Wirel. Commun*., vol. 21, no. 10, pp. 7990-8006, Oct. 2022.

[3] I. F. Akyildiz, J. M. Jornet, and C. Han, "Terahertz band: Next frontier for wireless communications," *Phys. Commun.*, vol. 12, pp.16-32, Sep. 2014.

[4] K. Guo, Y. Zhang and P. Reynaert, "A 0.53-THz subharmonic injection-locked phased array with 63-μW radiated power in 40-nm CMOS," *IEEE J. Solid-State Circuits*, vol. 54, no. 2, pp. 380-391, Feb. 2019.

[5] R. Klimovich, S. Jameson and E. Socher, "W-Band endfire 2-D phased-array transmitter based on ×9 CMOS active multiplier chips," *IEEE Trans. Antennas Propag.*, vol. 68, no. 12, pp. 7893-7904, Dec. 2020.

[6] K. Sato and Y. Monnai, "Terahertz beam steering based on trajectory deflection in dielectric-free Luneburg lens," *IEEE Trans. Terahertz Sci. Technol.*, vol. 10, no. 3, pp. 229-236, May 2020.

[7] G. -B. Wu, K. F. Chan, S. -W. Qu and C. H. Chan, "A 2-D beam-scanning Bessel launcher for terahertz applications," *IEEE Trans. Antennas Propag.*, vol. 68, no. 8, pp. 5893-5903, Aug. 2020.

[8] M. A. Campo, G. Carluccio, S. Bruni and N. Llombart, "Dielectric gratings enhancing the field of view in low dielectric permittivity elliptical lenses," *IEEE Trans. Antennas Propag.*, vol. 69, no. 11, pp. 7308-7322, Nov. 2021.

[9] M. K. T. Al-Nuaimi, S. -L. Zhu, W. G. Whittow, R. -S. Chen, G. -L. Huang and A. Mahmoud, "Design of Alvarez beam scanning reflectarray with inversely proportional focal length," *IEEE Antennas Wirel. Propag. Lett.*, vol. 22, no. 6, pp. 1416-1420, Jun. 2023.

[10] Z. Cao, Y. Li, Z. Zhang and M. F. Iskander, "Single motor-controlled mechanically reconfigurable reflectarray," *IEEE Trans. Antennas Propag.*, vol. 71, no. 1, pp. 190-199, Jan. 2023.

[11] H. Hasani, J. S. Silva, S. Capdevila, M. García-Vigueras and J. R. Mosig, "Dual-band circularly polarized transmitarray antenna for satellite communications at (20, 30) GHz," *IEEE Trans. Antennas Propag.*, vol. 67, no. 8, pp. 5325-5333, Aug. 2019.

[12] G. -B. Wu, S. -W. Qu and S. Yang, "Wide-angle beam-scanning reflectarray with mechanical steering," *IEEE Trans. Antennas Propag.*, vol. 66, no. 1, pp. 172-181, Jan. 2018.

[13] G. -B. Wu, S. -W. Qu, S. Yang and C. H. Chan, "Low-cost 1-D beam-steering reflectarray with ±70° scan coverage," *IEEE Trans. Antennas Propag.*, vol. 68, no. 6, pp. 5009-5014, Jun. 2020.

[14] Z. -Y. Yu, Y. -H. Zhang, S. -Y. He, H. -T. Gao, H. -T. Chen and G. -Q. Zhu, "A wide-angle coverage and low scan loss beam steering circularly polarized folded reflectarray antenna for millimeter-wave applications," *IEEE Trans. Antennas Propag.*, vol. 70, no. 4, pp. 2656-2667, Apr. 2022.

[15] E. B. Lima, S. A. Matos, J. R. Costa, C. A. Fernandes and N. J. G. Fonseca, "Circular polarization wide-angle beam steering at Ka-band by in-plane translation of a plate lens antenna," *IEEE Trans. Antennas Propag.*, vol. 63, no. 12, pp. 5443-5455, Dec. 2015.

[16] P. Nayeri, F. Yang and A. Z. Elsherbeni, "Bifocal design and aperture phase optimizations of reflectarray antennas for wide-angle beam scanning performance," *IEEE Trans. Antennas Propag.*, vol. 61, no. 9, pp. 4588-4597, Sept. 2013.

[17] Z. H. Jiang, Y. Zhang, J. Xu, Y. Yu, W. Hong, "Integrated broadband circularly polarized multibeam antennas using Berry-phase transmitarrays for Ka-band applications," *IEEE Trans. Antennas Propag.*, vol. 68, no. 2, pp. 859-872, Feb. 2020.

[18] P. -Y. Feng, S. -W. Qu and S. Yang, "Phased transmitarray antennas for 1-D beam scanning," *IEEE Antennas Wirel. Propag. Lett.*, vol. 18, no. 2, pp. 358-362, Feb. 2019.

[19] R. Xu and Z. N. Chen, "A compact beamsteering metasurface lens array antenna with low-cost phased array," *IEEE Trans. Antennas Propag*., vol. 69, no. 4, pp. 1992–2002, Apr. 2021.

[20] T. K. Pham, L. Guang, D. González-Ovejero and R. Sauleau, "Dual-band transmitarray with low scan loss for Satcom applications," *IEEE Trans. Antennas Propag*., vol. 69, no. 3, pp. 1775-1780, Mar. 2021.

[21] J. Hu, H. Wong and L. Ge, "A circularly-polarized multi-beam magneto-electric dipole transmitarray with linearly-polarized feeds for millimeter-wave applications," *IEEE Trans. Antennas Propag.*, vol. 70, no. 7, pp. 6012-6017, Jul. 2022.

[22] Á. F. Vaquero et al., "Design of low-profile transmitarray antennas with wide mechanical beam steering at millimeter waves," *IEEE Trans. Antennas Propag*., vol. 71, no. 4, pp. 3713-3718, Apr. 2023.

[23] P. Mei, G. F. Pedersen and S. Zhang, "Performance improvement of mechanically beam-steerable transmitarray antennas by using offset unifocal phase symmetry," *IEEE Trans. Antennas Propag.*, vol. 71, no. 1, pp. 1129-1134, Jan. 2023.

[24] L.-Z. Song, P.-Y. Qin, S.-L. Chen, Y. J. Guo, "An elliptical cylindrical shaped transmitarray for wide-angle multibeam applications," *IEEE Trans. Antennas Propag.*, vol. 69, no. 10, pp. 7023-7028, Oct. 2021.

[25] P. Wang, W. Ren, Q. Zeng, Z. Xue and W. Li, "Dual-band beam-scanning antenna at Ka-band by rotation of two transmitarrays," *IEEE Antennas Wireless Propag. Lett.*, vol. 21, no. 9, pp. 1792-1796, Sep. 2022.

[26] P. Mei, S. Zhang, and G. F. Pedersen, "A low-cost, high-efficiency and full-metal reflectarray antenna with mechanically 2-D beam-steerable capabilities for 5G applications," *IEEE Trans. Antennas Propag.*, vol. 68, no. 10, pp. 6997–7006, Oct. 2020.

[27] K. B. Ng, and C. H. Chan, "On the dielectric properties of substrates with different surface conditions for submillimeter-wave and terahertz applications," *THz Sci. Technol.*, vol. 9, no. 2, pp. 45-59, Jun. 2016.

[28] Q. Lou, C. Xue and Z. N. Chen, "High-efficiency metalens antenna using Huygens' metasurface with glide symmetric I-shape metal strips," *IEEE Trans. Antennas Propag.*, vol. 69, no. 11, pp. 7394-7403, Nov. 2021.

[29] L. -Z. Song, P. -Y. Qin and Y. J. Guo, "A high-efficiency conformal transmitarray antenna employing dual-layer ultra-thin Huygens element," *IEEE Trans. Antennas Propag.*, vol. 69, no. 2, pp. 848-858, Feb. 2021.